Implementation of Super High-speed Permanent Magnet Synchronous Machine Drive

Myoungho Kim†, Jung-Sik Yim†, Seung-Ki Sul†, Sung-Il Lim‡

†School of Electrical Engineering & Computer Science, Seoul National University
San 56-1, Shillim-Dong, Kwanak-Gu, Seoul, Korea
myoungho@eepel.snu.ac.kr

‡Turbo Machinery Development, Samsung Techwin Co., LTD
culsi.lim@samsung.com

***Abstract* -- This paper proposes the control algorithm for a Surface Mounted Permanent Magnet Synchronous Motor(SMPMSM) drive system running at 116,000 r/min. Hall sensors are employed to measure the rotor position, and a speed observer is used to enhance the dynamic performance of the drive system. And in order to extend the output power capacity in the high-speed operating region, a flux-weakening controller, integrated with an anti-windup controller, is implemented. Through the simulations and experiments, it is validated that both high speed operation and fast acceleration has achieved with the proposed methods.**

***Index Terms* -- Flux-weakening controller, Hall sensor, speed observer , super high-speed drive**

I. INTRODUCTION

Recently, super high-speed PMSM(Permanent Magnet Synchronous Motor) drives have become attractive in many applications such as micro-turbine generators, turbo compressors, and centrifuges because of their attractive features such as simple structure, light weight, small size and high efficiency compared to conventional high-speed drive systems[1]. As the super high-speed drives have distinguished its performance in industries, they have begun used in more various environments, and then some applications require more challenging specifications. Fast acceleration is one of the challenges. In order to develop a fast accelerating super high-speed system, however, two problems should be addressed.

One of the problems is how to measure or estimate the rotor position for the vector control; because position sensors such as resolvers and optical encoders may not be available due to mechanical vibration and temperature condition in the super high-speed systems. For this reason, a position sensorless vector control algorithm has been developed and used in industries[2]. However, the developed algorithm has poor accelerating performance due to the limited dynamic response of the position estimator. Hall sensors can be used in this case, but the system may suffer large current ripple and torque fluctuation due to the low resolution of the Hall sensors. Hence, there should be a measure for the low resolution problem of Hall sensors.

The other problem is the flux-weakening control during the fast acceleration. When the system accelerates extremely fast, a large amount of currents have to flow to the motor, and then the motor may operate in the flux-weakening region momentarily because of the lack of the available voltage to the motor. Therefore, an effective flux-weakening control should be incorporated with the speed and current regulators.

In this paper, Hall sensors together with a speed estimator is used to measure the rotor position and motor speed, and a flux-weakening controller, which is integrated with anti-windup controller, is employed. The proposed method is verified through computer simulation and experimental results.

II. SYSTEM DESCRIPTION

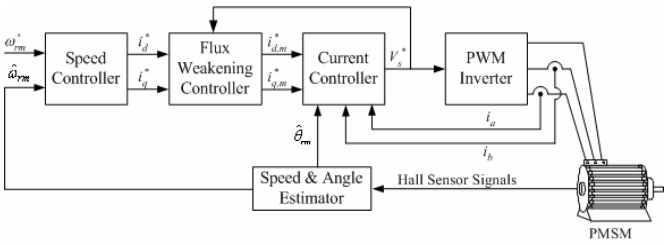

Fig. 1. Block diagram of developed system

Fig. 1 stands for the block diagram of the developed system in this paper. And the system parameters are presented in Table I. Both the speed and current regulators are composed of conventional Proportional and Integral (PI) type regulator[3]; the regulators are digitally implemented using high-performance DSP. And a Pulse Width Modulation (PWM) Voltage Source Inverter (VSI) is used as a power conversion device.

The developed system employs three Hall sensors to acquire the rotor position, and a speed estimator is added to overcome the low resolution problem of Hall sensors, In addition, a flux-weakening controller, which modifies the current references using the output voltage information of the current regulator, is also implemented. The details of speed

estimator and the flux-weakening controller are explained in the next sections.

TABLE I. System Parameters

Motor type	SMPMSM
Number of poles	2
Maximum operating speed	116,000 *r/min*
Sampling frequency	30 *kHz*
Switching frequency	15 *kHz*
Current regulator bandwidth	1 *kHz*
Speed regulator bandwidth	10 *Hz*

III. Position and Speed Estimation

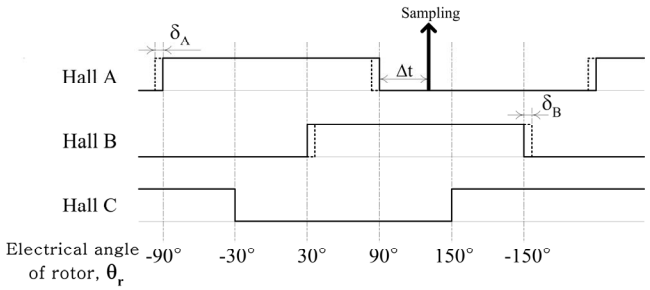

Fig. 2. Output signals of Hall sensors
Solid line: The ideal output waveform
Dotted line: The output waveform with Hall sensor misalignments

Fig. 2 shows the output signals of Hall sensors. Three Hall sensors are installed 120º apart each other, and the position measurement is updated six times per one electric revolution. Hence, the resolution of the measured rotor position is 60 º, which is large enough to make large current ripples. For this reason, interpolation is generally used; the motor speed, ω_{r_hall}, and rotor position, θ_{r_hall}, between the Hall sensor signals can be calculated using the pulse transition time, Δt_{hall}, and the Hall sensor angle, θ_{hall}, as follows,

$$\omega_{r\_hall} = \frac{\pi}{3} / \Delta t_{hall}\,, \tag{1}$$

$$\theta_{r\_hall} = \theta_{hall} + \omega_{r\_hall} \cdot \Delta t\,, \tag{2}$$

where Δt is the time between the calculating point and the last Hall sensor update point as shown in Fig. 2. However, the interpolated motor speed and rotor position have some errors when the motor speed varies. In addition, even in the constant speed operation, ω_{r_hall} and θ_{r_hall} contains harmonics of the electric rotating speed due to the mechanical misalignment of the Hall sensors, which is presented as δ_A and δ_B in Fig. 2. Such errors deteriorate severely the performance of motor control[4] and may result in the instability of the control system, especially at higher operating speed.

In order to validate the effect of the Hall sensor misalignment, simulations are performed; in the simulations, the magnitude of the misalignment, δ_A and δ_B, is set to 10˚. Fig. 3 (a) and (b) are the simulation results of steady state operation when the motor speed is, 116,000 *r/min,* constant but with the specified Hall sensor misalignments. Fig. 3 (a) shows the real rotor position, θ_{real}, calculated position, θ_{r_hall}, and Hall sensor output, θ_{hall}. Fig. 3 (b) shows the real rotor speed, ω_{rm} , and calculated rotor speed, ω_{rm_hall}. From Fig. 3 (a) and (b), it can be seen that the interpolated motor speed and rotor position fluctuate due to the Hall sensor misalignment; and the magnitude of the speed fluctuation is approximately 4,000 *r/min*. This results mean that the interpolated speed can not follow the real speed correctly.

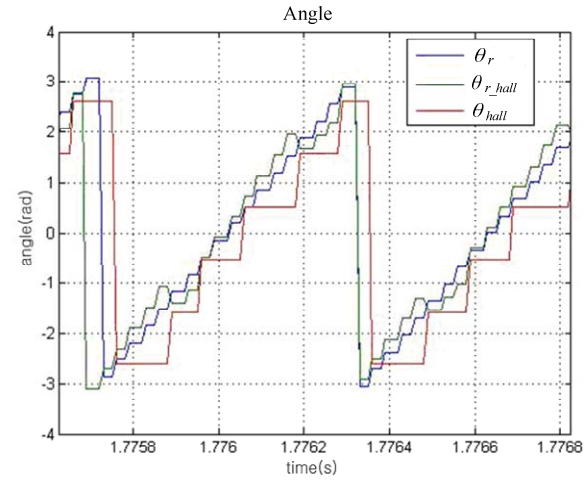

(a) Real angle, calculated angle and Hall sensor output

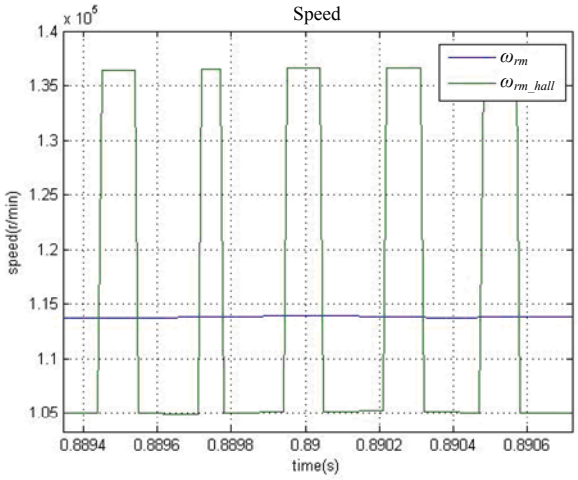

(b) Real speed and calculated speed

Fig. 3. Simulation result of 116,000 *r/min* operation with Hall sensor misalignment errors

In order to suppress the fluctuations described above, a closed-loop speed estimator is employed. The differential equation of the mechanical system can be expressed as follows,

$$T_e = J_m \frac{d\omega_{rm}}{dt} + T_L, \tag{3}$$

and its state-space equation can be described,

$$\begin{bmatrix} \dot{\omega}_{rm} \\ \dot{\theta}_{rm} \end{bmatrix} = \begin{bmatrix} -\frac{1}{J_m} & 0 \\ 0 & 1 \end{bmatrix} \cdot \begin{bmatrix} \omega_{rm} \\ \theta_{rm} \end{bmatrix} + \begin{bmatrix} \frac{1}{J_m} \\ 0 \end{bmatrix} \cdot T_e, \tag{4}$$

where the rotor position is θ_{rm} and the motor speed is ω_{rm}. Then, a closed-loop speed estimator can be implemented as follows,

$$\begin{bmatrix} \dot{\hat{T}}_L \\ \dot{\hat{\omega}}_{rm} \\ \dot{\hat{\theta}}_{rm} \end{bmatrix} = \begin{bmatrix} 0 & 0 & 0 \\ -\frac{1}{J_m} & 0 & 0 \\ 0 & 1 & 0 \end{bmatrix} \cdot \begin{bmatrix} \hat{T}_L \\ \hat{\omega}_{rm} \\ \hat{\theta}_{rm} \end{bmatrix} + \begin{bmatrix} 0 \\ \frac{1}{J_m} \\ 0 \end{bmatrix} \cdot T_e + \begin{bmatrix} k_1 \\ k_2 \\ k_3 \end{bmatrix} \cdot \left(\theta_{hall} - \hat{\theta}_{rm}\right), \tag{5}$$

where the estimated rotor position is $\hat{\theta}_{rm}$, the estimated motor speed is $\hat{\omega}_{rm}$, and the estimated load torque is $\hat{T}_L$. And the block diagram of the estimator can be presented as Fig. 4[5].

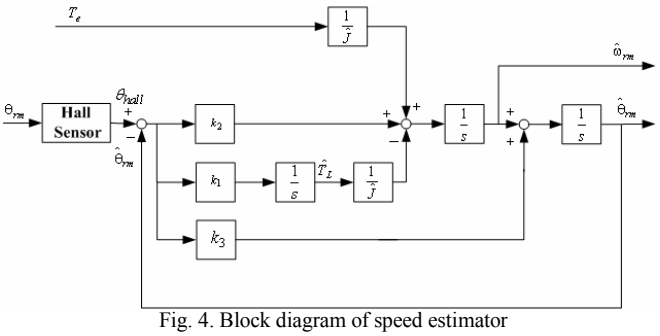

Fig. 4. Block diagram of speed estimator

As shown in the equation (5) and Fig. 4, it can be noticed that the difference between θ_{hall} and $\hat{\theta}_{rm}$ is used as the position error in the estimator. And then, the transfer functions of the estimator can be expressed as follows,

$$\left.\frac{\hat{\theta}_{rm}}{\theta_{hall}}\right|_{T_e=0} = \frac{k_3 \cdot s^2 + k_2 \cdot s - \frac{k_1}{\hat{J}_m}}{s^3 + k_3 \cdot s^2 + k_2 \cdot s - \frac{k_1}{\hat{J}_m}}, \tag{6}$$

$$\left.\frac{\hat{\omega}_{rm}}{\theta_{hall}}\right|_{T_e=0} = \frac{s \cdot \left(k_2 \cdot s - \frac{k_1}{\hat{J}_m}\right)}{s^3 + k_3 \cdot s^2 + k_2 \cdot s - \frac{k_1}{\hat{J}_m}}, \tag{7}$$

when T_e is assumed to be ignored. From (6) and (7), it can be found that the two transfer functions are similar to the transfer function of low-pass filter. Therefore, the fluctuation due to the low resolution and the misalignment of the Hall sensors can be filtered out if the equivalent cut-off frequency

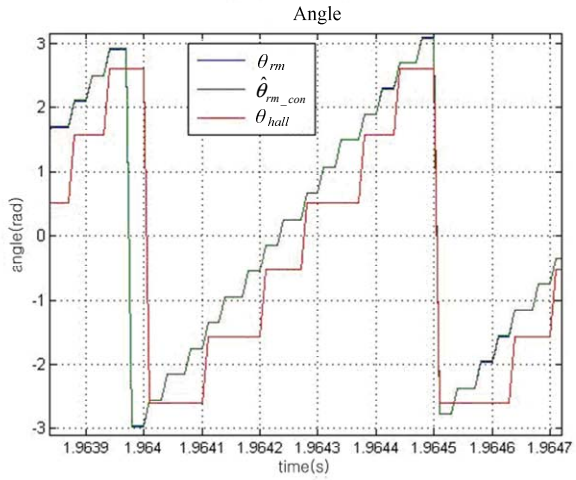

(a) Real angle, calculated angle and Hall sensor output

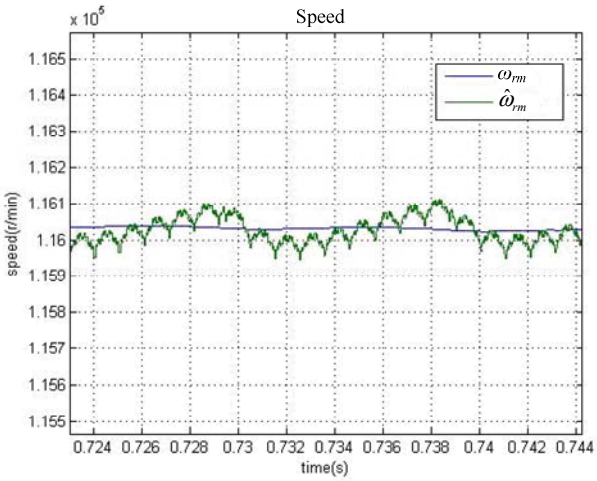

(b) Real speed and estimated speed

Fig. 5. Simulation result of 116,000 *r/min* operation with Hall sensor misalignment errors, using the speed estimator

of (6) and (7) is low enough compared the rotating frequency of SMPMSM,. Noting that the speed estimator has a feed-forward input of T_e, the equivalent cut-off frequency does not affect the dynamic response of $\hat{\theta}_{rm}$ and $\hat{\omega}_{rm}$ as far as the parameter errors are negligible.

However, the steady state error in $\hat{\theta}_{rm}$ should be compensated. The estimated angle passes through middle of θ_{hall}'s step and the pulse width between the hall sensor signals is 60°; therefore there exists an offset of 30° in the estimated angle. This offset simply can be compensated as follows,

$$\hat{\theta}_{rm\_con} = \hat{\theta}_{rm} + \frac{\pi}{6}, \tag{8}$$

where $\hat{\theta}_{rm}$ is the angle computed by the estimator and $\hat{\theta}_{rm\_con}$ is the angle used for the vector control.

Fig. 5 (a) and (b) present the simulation results using the speed estimator. The magnitude of the misalignment is 10˚, same to the previous simulation. The gains of the estimator are selected to locate the poles of (6) and (7) at 50*Hz*. As shown in Fig. 5 (a), real and estimated angle are nearly overlapped, and interpolate the hall sensor signal quite well regardless of the misalignments. And as shown in Fig. 5 (b), the harmonics in the estimated speed is suppressed well by the estimator; the speed ripple is less than 0.1% of the real motor speed.

IV. FLUX-WEAKENING CONTROL METHOD

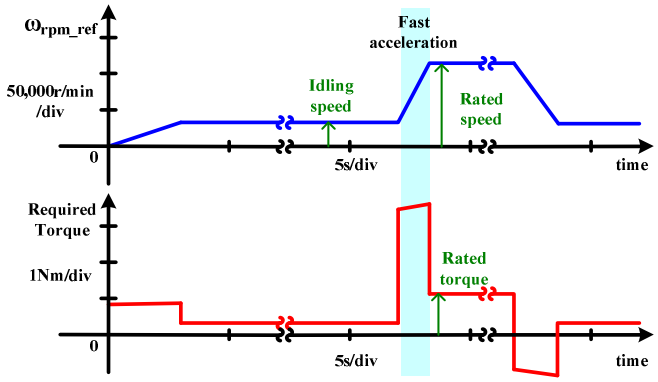

Fig. 6. Speed profile and required torque of the developed system

The target speed profile and required acceleration torque of the developed system is presented in Fig. 6. As shown in Fig. 6, the maximum acceleration torque is larger than two times of the rated torque. As a result, the motor should be overloaded for the fast acceleration period, and then the operating point moves to the flux-weakening region because of the lack of the available voltage to the motor.

Fig. 7 (a) and (b) show the flux-weakening control strategy used in this paper. The current trajectory of the flux-weakening control is presented in Fig. 7 (a). When SMPMSM is accelerated according to the given speed profile, the current reference increases over the rated current limit circle; the current reference is located at the intersection point of the instantaneous current limit circle and the voltage limit circle, which is the flux-weakening region 1 and presented as the operating point B and C in Fig. 7 (a). As the speed of the motor increases, the available terminal voltage is not large enough to run the motor at the operating point C in the fast acceleration period. Because of the voltage limit, the operating point moves from C to D, which lies in the flux-weakening region 2, as the speed approaches to the rated value. After the acceleration, the current is limited within the rated value in the steady state, and the system returns to the flux-weakening region 1 which is shown as the operating E[6].

In this paper, a flux-weakening controller integrated with an anti-windup controller is employed[7]. The block diagram of the flux-weakening controller is presented in Fig. 7 (b). When the motor is driven in the flux-weakening area as the speed increases, the output voltages of the current regulator, v_{dqs}^{r*}, becomes different from those of the inverter, v_{dqs}^{r}, because of the voltage limitation of the inverter. Then these voltage differences are low-pass filtered, and the flux-weakening controller moves the d-axis current reference, i_{ds}^{r*}, toward negative direction using the filtered values. And the q-axis current reference, i_{qs}^{r*}, is limited by the modified d-axis current reference, $i_{ds\_m}^{r*}$, in order to limit the whole current within the instantaneous current limitation. The feedback path with the high-pass filter is implemented to keep the controller less sensitive to the sudden change of q-axis current; and the blocks in the dotted box is for the Maximum Torque Per Voltage (MTPV) operation at the flux-weakening region 2.

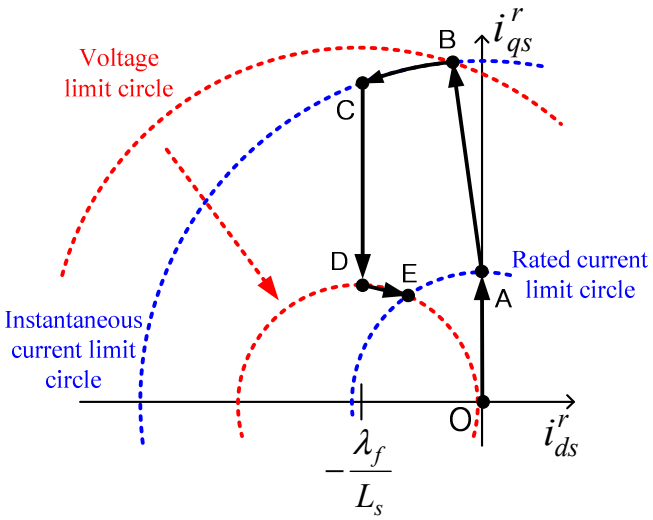

(a) Voltage and current limit and operating points

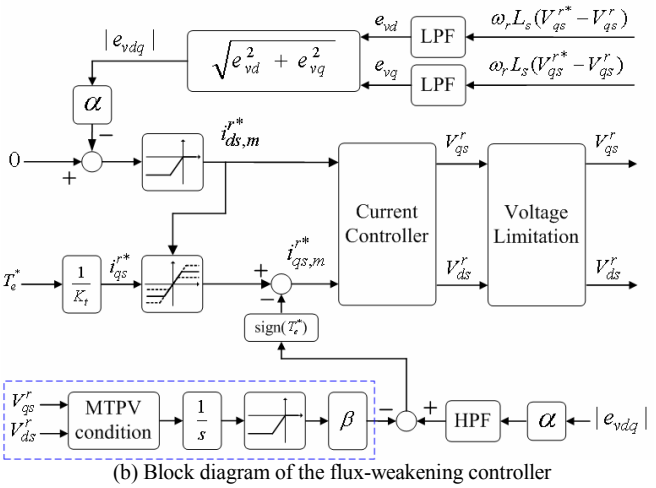

(b) Block diagram of the flux-weakening controller

Fig. 7. Flux-weakening control strategy

Noting that the voltage differences are commonly used for the anti-windup controller, this method is designed to have the ability of the flux-weakening control and anti-windup at the same time.

V. Experimental Results

The experimental results with the speed estimator and flux-weakening controller at the speed of 112,100 *r/min* are presented in Fig. 8 (a) and (b). Fig. 8 (a) shows the calculated speed, ω_{r_hall}, estimated speed, $\hat{\omega}_{rm}$, Hall sensor output, θ_{hall}, and estimated angle, $\hat{\theta}_{rm\_con}$. In the experiment, the three poles of the estimator are located at 50 *Hz*. As shown in Fig. 8 (a), each step of θ_{hall} has different time duration due to the Hall sensor misalignment. And in addition, ω_{r_hall} has speed ripples because of the misalignment; the ripple frequency is same as the rotating frequency and the magnitude is 4.3% of the motor speed. However, the speed ripple is conspicuously reduced in $\hat{\omega}_{rm}$; the magnitude is reduced to 0.07% of the motor speed with the speed estimator.

In Fig. 8 (b), d- and q-axes currents during the fast acceleration and deceleration are presented. In the experiments, the motor speed is increased from 29,500r/min to 112,100r/min in 1.2s. As shown in Fig. 8 (b), the operating point moves through the flux-weakening region 1 and 2 during the acceleration and returns to flux-weakening region 1 after the acceleration. These results show that flux weakening control is performed consistently with the implemented controller.

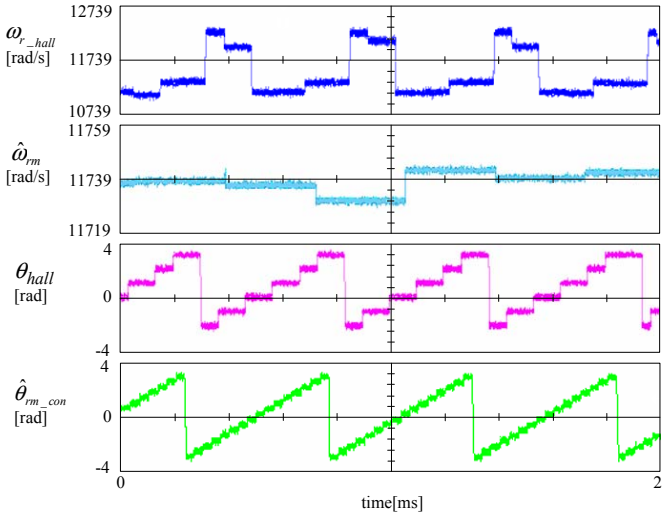

(a) Speed calculated using Hall sensors and the speed estimator, Hall sensor output and estimated angle

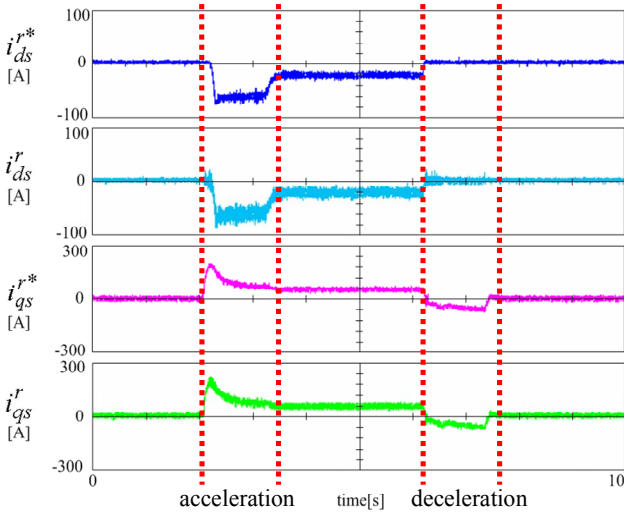

(b) D-q axes currents and references on acceleration and deceleration

Fig. 8. Experimental results in the steady state and in the transient state

VI. Conclusion

In this paper, a super high-speed SMPMSM drive system equipped with Hall sensors has been developed. Because of its higher operating speed and fast acceleration rate, a speed estimator and a flux-weakening controller have been devised. The Hall sensor signal is interpolated using the speed estimator and the speed ripples are remarkably reduced even with the reasonable Hall sensor misalignments. The flux-weakening controller modifies current references using output voltages of the current regulator according to the operating condition. Developed system is validated by the simulation and the experimental result.

References

[1] M.A.Rahman, Akira Chiba, Tadashi Fukao, "Super High Speed Electrical Machines Summary,"in Power Engineering Society General Meeting, IEEE vol. 2, 2004, pp. 1272-1275

[2] Bon-Ho Bae, Seung-Ki Sul, Jeong-Hyeck Kwon, Ji-Seob Byeon, "Implementation of sensorless vector control for super-high-speed PMSM of turbo-compressor,"IEEE Tans. Ind. Applicat., vol. 39, pp. 811-818, May-June 2003.

[3] D. W. Novotny and T.A Lipo, *Vector Control and Dynamics of AC Machines*, New York: Oxfrd, 1996, ch.5.

[4] Beccue. P.B., Pekarek. S.D., Deken. B.J., Koenig. A.C., "Compensation for Asymmetries and Misalignment in a Hall-Effect Position Observer Used in PMSM Torque-Ripple Control," IEEE Trans. Ind. Applicat., vol. 43, pp. 560-570, March-April 2007.

[5] H. Kim et al., "A New Motor Speed Estimator Using Kalman Filter in Low-Speed Range," IEEE Trans. on Ind. Appl., vol.43, pp. 498-504, August 1996.

[6] S. Morimoto, Y. Takeda, T. Hirasa, and K. Taniguchi, "Expansion of Operating Limits for permanent magnet motor by current vector control considering inverter capacity," IEEE Trans. Ind. Applicat., vol. 26, pp. 866-871, Sept./Oct., 1990.

[7] Tae-Suk Kwon and Seung-Ki Sul, "Novel Antiwindup of a Current Regulator of a Surface-Mounted Permanent-Magnet Motor for Flux-Weakening Control," IEEE Trans. on Ind. Appl., vol.42, pp. 1293-1300, September-October 2006.